VOLUME 8, NUMBER 8, AUGUST 2008

NANO LETTERS

Strong Suppression of Electrical Noise in Bilayer Graphene Nanodevices

Yu-Ming Lin* and Phaedon Avouris

IBM T. J. Watson Research Center, Yorktown Heights, New York 10598

Received January 24, 2008; Revised Manuscript Received February 6, 2008

ABSTRACT

Low-frequency 1/*f* noise is ubiquitous and dominates the signal-to-noise performance in nanodevices. Here we investigate the noise characteristics of single-layer and bilayer graphene nanodevices and uncover an unexpected 1/*f* noise behavior for bilayer devices. Graphene is a single layer of graphite, where carbon atoms form a two-dimensional (2D) honeycomb lattice. Despite the similar composition, bilayer graphene (two graphene monolayers stacked in the natural graphite order) is a distinct 2D system with a different band structure and electrical properties.[1,2] In graphene monolayers, the 1/*f* noise is found to follow Hooge's empirical relation with a noise parameter comparable to that of bulk semiconductors. However, this 1/*f* noise is strongly suppressed in bilayer graphene devices and exhibits an unusual dependence on the carrier density, different from most other materials. The unexpected noise behavior in graphene bilayers is associated with its unique band structure that varies with the charge distribution among the two layers, resulting in an effective screening of potential fluctuations due to external impurity charges. The findings here point to exciting opportunities for graphene bilayers in low-noise applications.

Ultrathin graphite films have attracted strong scientific and technological interest as truly two-dimensional (2D) transport systems[3–5] with exceptional carrier mobilities.[6,7] While a single-layer 2D graphene is a zero-gap semiconductor, which is not suitable for certain applications, a wealth of different band structures emerges in nanoscale graphene that exhibit band gaps and distinct electrical properties[8] desirable for various device applications, such as metallic interconnects,[7] field-effect transistors,[9,10] and single-charge devices.[4] In addition, both experimental[9,11] and theoretical[12] studies have shown that the transport properties of graphene systems are highly sensitive to external perturbations such as adsorbed molecules on the surface or nearby impurity charges, indicating that graphene is also advantageous for sensor applications.[13] However, this high sensitivity of graphene devices also implies that any uncontrolled and random perturbations in the environment would lead to significant device current fluctuations and contribute to low-frequency 1/*f* noise. We note that while 1/*f* noise is ubiquitous in solid-state electronic devices, this type of noise is of particular significance in determining and/or limiting the performance for nanoscale devices because its amplitude always increases with diminishing device dimensions. Moreover, for high-frequency applications where graphene holds great potential because of its high mobility, this low-frequency noise can be up-converted to induce phase noise in rf designs[14] and affect device performance. Despite the broad interest and intense experimental focus on graphene, a comprehensive study on the noise characteristics of graphene devices is still lacking.

Here we report on the fabrication and investigation of the electrical noise characteristics of two-terminal single-layer graphene (SLG) and bilayer graphene (BLG) nanodevices. Structurally, carbon nanotubes are considered as a special case of rolled-up graphene nanoribbons, and therefore, much of the knowledge acquired from the extensive studies on carbon nanotubes may be readily applied here to shed light

* Corresponding author: yming@us.ibm.com.

10.1021/nl080241l CCC: $40.75
Published on Web 02/26/2008

on the understanding of experimental results. The behavior of 1/*f* noise in single-walled carbon nanotube devices has been systematically studied previously, and it is found that the origin of 1/*f* noise in these nanodevices is dominated by fluctuations of trap charges in the oxide.[15,16] The noise level in carbon nanotube devices can be lowered by improving the oxide quality through passivation[17] and/or thermal annealing[18] or by removing the oxide entirely.[19] In these efforts, the noise reduction is due to the elimination of trap charges, regardless of the properties of the transport channel. In this report, we demonstrate a different approach to reduce 1/*f* noise in graphene devices, as illustrated by the strong suppression of 1/*f* noise in graphene bilayers compared to single-layer graphene and nanotube devices, all in the presence of similar oxide quality. This unexpected noise behavior in graphene bilayers is associated with its unique band structure that varies with the charge distribution among the two layers, resulting in an effective screening of potential fluctuations associated with external impurity charges. These results not only point to exciting opportunities for graphene bilayers in low-noise applications but also provide valuable insight for further noise reduction in nanodevices.

Figure 1A shows a scanning electron microscopy (SEM) image of the graphite flake used in this study, where regions with different numbers of graphene layers can be readily identified from the image brightness. Figure 1B shows the trace of the atomic force microscopy (AFM) height profile measured along the arrow in Figure 1A, corresponding to regions with mono-, bi-, and trilayer graphene. The inset of Figure 1C shows an SEM image of a graphene nanoribbon device with a channel width of 30 nm, following fabrication methods reported previously.[9,10] We have also performed Raman spectroscopy measurements to confirm the number of graphene layers shown here.

With the underlying Si substrate as the gate electrode, Figure 1C shows the device resistance as a function of gate voltage for two SLG and BLG devices with identical channel geometry (see inset). We note that both devices exhibit a Dirac point corresponding to the resistance maximum near $V_g = 0$, indicating insignificant doping effects in the fabrication process. Compared to SLG nanodevices, the BLG device of the same geometry always possesses a lower channel resistance and a weaker gate dependence. For example, in Figure 1C, BLG and SLG devices exhibit comparable resistance values at either sufficiently large or negative gate voltages ($V_g \sim \pm 20$ V), whereas the resistance of the SLG device is more than three times higher than that of the BLG at the Dirac point. The fact that the resistance ratio of the SLG and BLG devices is not a constant as a function of V_g clearly demonstrates that carrier transport in BLG devices cannot simply be regarded as two noninteracting graphene layers placed in parallel. Instead, the stacking order in bilayer graphene leads to a different 2D dispersion relation from that of SLG, which should be used to describe the transport properties in BLG. We also note that in Figure 1C, the resistance maximum of the BLG device is less than half of their SLG counterpart, consistent with theoretical calculations that predict a resistance ratio as large as 6 at the Dirac point for the two cases in the weak-disorder limit.[20,21]

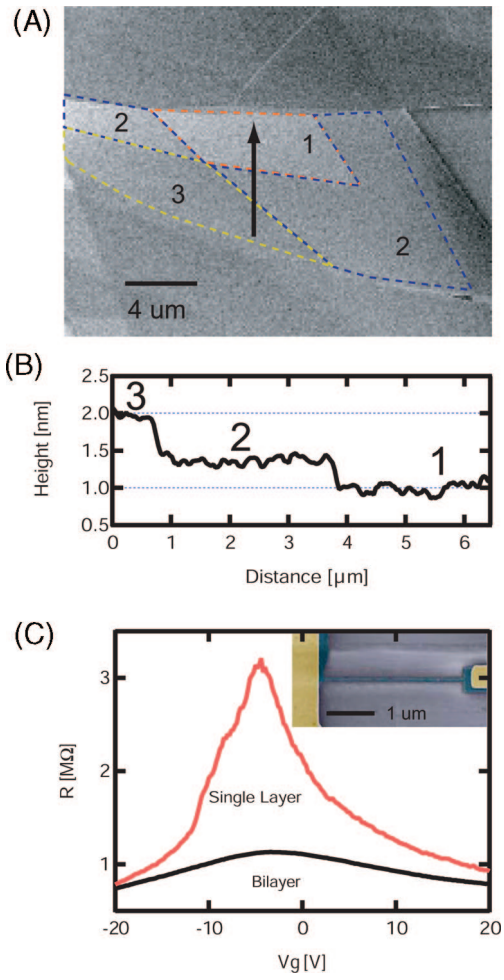

Figure 1. Identification of single-layer and bilayer graphene regions and device fabrication. (A) SEM image of a graphite flake deposited on the SiO_2/Si surface. The contrast of the image brightness reflects segments corresponding to different layer thicknesses, as indicated by the number of layers in the figure. Single-layer and bilayer nanodevices in this study are fabricated using the top and bottom graphene demains labeled by 1 and 2, respectively. (B) Trace of the height profile measured by AFM along the arrow shown in Figure 1A, yielding a height difference ≤5 Å for each layer. (C) Resistance of one single-layer and one bilayer graphene nanoribbon devices measured as a function of gate voltage. The two devices possess identical channel layout ($W = 30$ nm and $L = 2.8$ μm) as shown in the inset.

In addition to the different gate dependence, a closer examination of Figure 1C reveals that the measured $I-V_g$ curve of the BLG device is much smoother than that of the SLG device, an intriguing observation for two nanodevices having the same dimensions and comparable resistance. In order to quantitatively study and compare these current fluctuations, we use a spectrum analyzer to measure the current power spectra at a dc bias, and at first we focus on a SLG device with a channel width W of 30 nm and length L of 1.7 μm. The inset of Figure 2A shows the measured current power spectral density S_I as a function of frequency (f) of the SLG device at a bias $V_d = 100$ mV for two different gate voltages. The power spectral density is found to be proportional to the current square I^2 in the linear $I-V_d$ regime

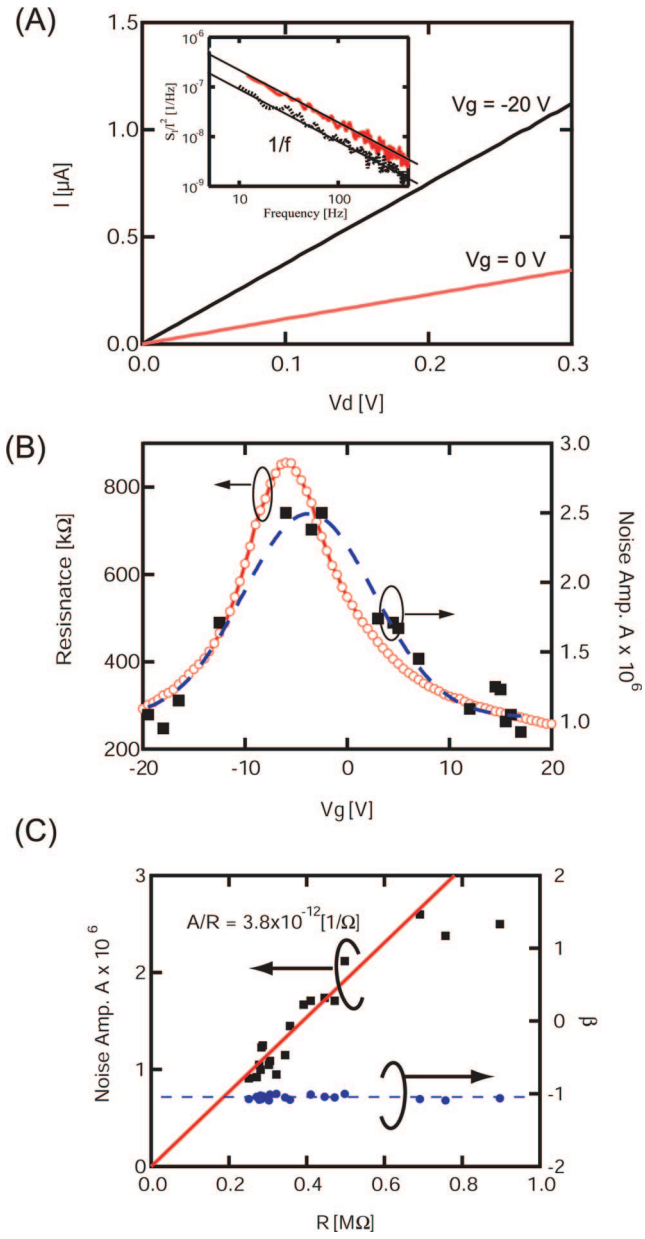

Figure 2. Electrical transport and noise characterization of a single-layer graphene nanoribbon device. (A) Device current as a function of drain voltage of a SLG nanoribbon device at $V_g = 0$ and -20 V, showing the excellent linear dependence. The inset shows the noise power spectra density S_I, normalized by I^2, as a function of frequency (f) for two gate voltages. The noise power spectrum at both gate voltages follows the f^{-1} dependence, as indicated by the solid lines, and is called the $1/f$ noise. Note that at $V_g = -20$ V the device exhibits a smaller resistance as well as a lower noise level S_I/I^2 (dashed curve in the inset). (B) The resistance and the noise amplitude A_N, defined in eq 1, of the SLG nanoribbon device measured as a function of gate voltage. The dashed curve is a guide to the eye, illustrating the correlation between A_N and R. (C) The noise amplitude A_N and the frequency exponent β of the SLG device plotted as a function of resistance. The frequency exponent $\beta \sim -1$ confirms the $1/f$ noise behavior for the gate voltage range studied and, thus, ensures the validity of the obtained A_N. The solid line is a linear fit of A_N vs R, yielding good agreement with Hooge's empirical relation.

and inversely proportional to the frequency (see Figure 2A). This frequency dependence is characteristic of the so-called $1/f$ noise, which is the dominant low-frequency noise existing in essentially all electronic materials. The current power spectra can be expressed as

$$S_I = A_N I^2 f^{\beta} \tag{1}$$

where β is the frequency exponent with a value close to -1, to within ± 0.1, and A_N is the $1/f$ noise amplitude. We note that this $S_I \propto I^2$ dependence in the linear $I-V_d$ curve shown in Figure 2A indicates that the $1/f$ noise in SLG is due to resistance fluctuations, i.e., $S_R/R^2 = S_I/I^2$.[15]

The noise amplitude A_N of the SLG device is found to be dependent on the gate voltage, as illustrated by Figure 2A, which shows a weaker noise spectrum, S_I/I^2, for a gate voltage corresponding to a lower-resistance state. Figure 2B plots the device resistance, R, and the noise amplitude,A_N, as a function of V_G, showing a positive correlation between these two quantities. In order to understand this $1/f$ noise behavior, we compare the SLG device with a single-wall carbon nanotube (CNT) device; in terms of transport, both can be visualized as a ribbon of single-layer graphene with a finite and narrow width. The noise characteristics of individual nanotube devices have been studied previously,[15,16] and their noise power spectrum is also described by eq 1. In semiconducting nanotubes, the noise amplitude A_N exhibits a strong gate dependence by more than 2 orders of magnitude and A_N is found to follow the empirical relation $A_N = \alpha_H/N$, called Hooge's relation,[22] where N is the total number of transport carriers in the device channel and α_H is defined as Hooge's noise parameter. It is important to point out that this noise parameter α_H, while assumed constant for a given device or material, is not an absolute constant and, instead, is often used as a technological measure for electronic device and/or materials quality. For nanotube devices fabricated on a SiO_2 surface, α_H is roughly $\sim 10^{-3}$, and its exact value is determined by the gate oxide quality.[19] We note that since the resistance of SLG devices is inversely proportional to the carrier density, the fact that the measured resistance R and noise amplitude A_N curves possess nearly identical gate dependence (see Figure 2B), provides strong evidence that the $1/f$ noise behavior follows Hooge's relation in single-layer graphene samples, as in the case of CNTs.

From Hooge's relation for A_N and the resistance of SLG devices given by $R = (en\mu)^{-1}(L/W)$, we find

$$A_N/R = \left(\frac{e\mu}{L^2}\right)\alpha_H \tag{2}$$

where μ is the carrier mobility and L is the device channel length. To calculate the mobility, we utilize the gate-dependent conductance along with the relation $n = \gamma V_g$ (where $\gamma \approx 7.2 \times 10^{10}$ cm^{-2} /V for a 300 nm SiO_2 layer[3,6]) and obtain a field-effect carrier mobility $\mu \sim 700$ cm^2 /V s for the 30 nm wide SLG device shown in Figure 2B. In Figure 2C, we plot the noise amplitude A_N as a function of resistance, showing a linear dependence in agreement with Hooge's relation. On the basis of the fitted slope $A_N/R = 3.8 \times 10^{-12}(1/\Omega)$ in Figure 2C, Hooge's noise parameter of the SLG device is found to be $\alpha_H \sim 1 \times 10^{-3}$ (see eq 2). To ensure the validity of this noise analysis for graphene, Figure 2C also shows the power exponent β of the noise power spectra as a function of device resistance, confirming the $1/f$

dependence for all gate voltages. Although it may not be unexpected that both single-wall CNT and single-layer graphene devices possess similar 1/*f* noise characteristics described by Hooge's relation and yield comparable noise parameters α_H in the range of 10^{-3}, these are importance findings with significant implications. First, despite different contact configurations (ohmic in SLG[4] vs Schottky barrier in CNT[23]), these results clearly suggest that in both systems the 1/*f* noise is dominated by the presence of the underlying oxide, where trapping/detrapping processes are expected to be the major sources for the 1/*f* noise. In particular, the quantitatively similar noise behavior in the two systems may arise from the similar configuration where the electrical transports are entirely carried by mobile charges that are in direct contact with the same oxide layer. There is, however, an important difference between the SLG nanoribbon and the CNT devices associated with the edge states at the channel boundary in the graphene nanoribbon, which has been shown to affect its transport properties and lead to a lower mobility in nanoribbon devices than that of their unpatterned counterparts.[9] However, since both CNT and SLG devices yield comparable α_H values, these uncontrolled edge states do not seem to affect the 1/*f* noise in graphene nanoribbons. In addition, the symmetry of the noise amplitude and resistance with respect to *n* and *p* branches (see Figure 2B), where the resulting A_R-R data sets can be nicely fitted by one single slope, indicates that the processes responsible for the 1/*f* noise do not depend on the type of transport carrier.

Next, we examine the noise characteristics of a bilayer graphene nanodevice with the same channel width $W = 30$ nm and a length $L = 2.8$ μm. As shown in Figure 3A, the BLG device also exhibits linear $I-V_d$ characteristics and current fluctuations with a 1/*f* frequency dependence (see inset). In Figure 3A, one important observation is that the 1/*f* noise amplitude of the BLG is found to be higher for the gate voltage corresponding to a lower-resistance state, in sharp contrast to the SLG device (see Figure 2A). In Figure 3B, we plot the measured resistance and noise amplitude of the BLG device as a function of V_g, showing a strikingly different noise behavior from that of SLG devices. In Figure 3B, the noise amplitude A_N is minimal at the Dirac point and increases with decreasing resistances, whereas in a SLG device, A_N is at its maximum near the Dirac point (see Figure 2B). Figure 3C shows the noise amplitude A_N versus the resistance of the BLG device, displaying this distinct inverse correlation between A_N and *R*. It is important to note that for most bulk semiconductor materials, if not all, the noise amplitude A_N is found to rise with increasing resistance under field-effect modulation. Qualitatively, this is attributed to the relatively weak dependence of the fluctuation mechanism responsible for the noise compared to the carrier density modulation due to the field-effect gating. To the best of our knowledge, the noise dependence of BLG devices shown here (see Figure 3C) is distinct from that of other known electrical systems including carbon nanotubes, and this unique phenomenon must be associated with the unusual band structure of the bilayer graphene. In addition to the different gate dependence, the 1/*f* noise amplitude A_N of the BLG device, ranging between 1–2 $\times$ 10^{-7} (see Figure 3B), is significantly smaller than that of the SLG device ($\geq 10^{-6}$

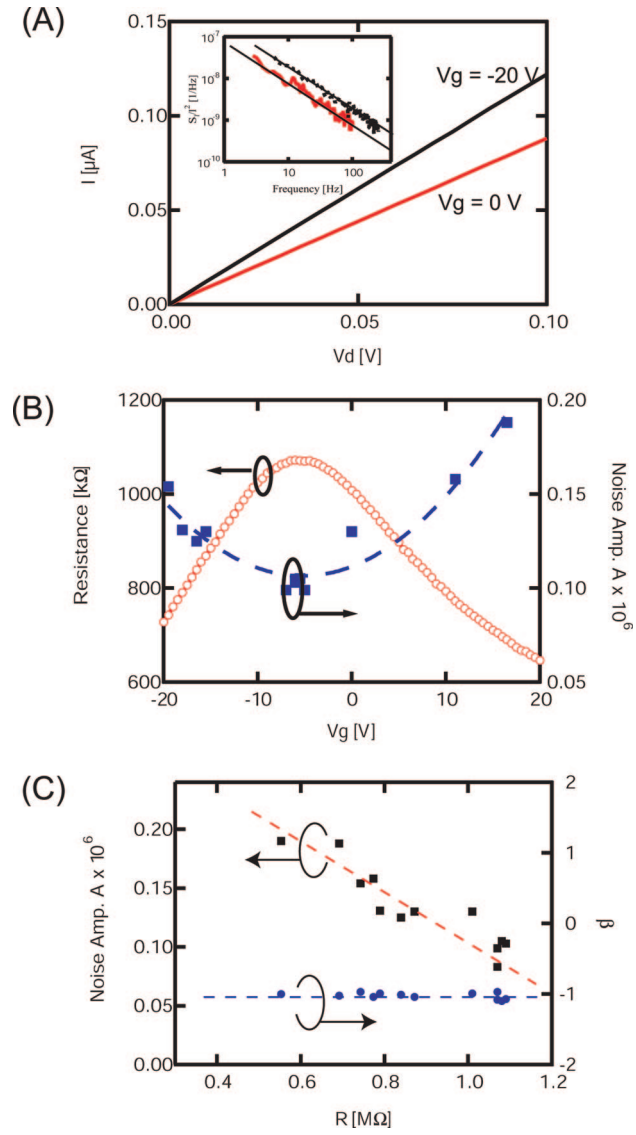

Figure 3. Electrical transport and noise characterization of a bilayer graphene nanoribbon device. (A) Device current as a function of drain voltage of a BLG nanoribbon device at $V_g = 0$ and -20 V, showing the linear dependence. The inset shows noise power spectra S_I/I^2 as a function of frequency for these two gate voltages. At $V_g = -20$ V, the BLG device possesses a smaller resistance, but exhibits a higher noise level (dashed curve in the inset), which is in contrast to the case of a SLG device shown in Figure 2A. (B) The resistance and the noise amplitude A_N of the BLG device measured as a function of gate voltage. The dashed curve is a guide to the eye, illustrating the inverse relation between A_N and *R*. (C) The noise amplitude A_N and the frequency exponent β of the SLG device as a function of resistance. While the frequency exponent still yields the expected $\beta \simeq -1$, the noise amplitude A_N increases with decreasing *R*, in drastic contrast to the SLG device shown in Figure 2C. The dashed line on A_N is a guide to the eye to highlight this difference.

in Figure 2B), even after taking into account the factor of ~2.7 due to the length difference. This lower A_N is consistent with the smoother $I-V$ curves of the BLG device shown in Figure 1C.

To further analyze the 1/*f* noise characteristics observed in SLG and BLG devices, we have fabricated and characterized both types of devices with different channel dimensions,

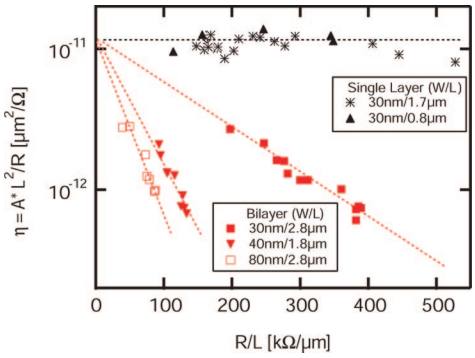

Figure 4. Comparison of the noise characteristics of SLG and BLG devices. The measured noise factor η, defined as $A_N L^2/R$, as a function of unit-length resistance for two SLG and three BLG devices with different channel dimensions. Both SLG devices shown here exhibit a nearly constant noise factor η as the resistance varies, in consistent with Hooge's relation, and yield $\alpha_H \sim 10^{-3}$. In contrast, all three BLG devices possess a much lower noise factor η than that of SLG devices. Moreover, these BLG devices possess a noise factor η that rises with decreasing resistance, which can be phenomenologically described by eq 3.

all showing the same trends discussed above (see Figure 4). We note that while the unusual noise behavior in bilayer graphene does not necessarily exclude the validity of Hooge's relation for this system, the noise parameter α_H cannot be unambiguously obtained in this context using eq 2. Therefore, to compare the noise level of graphene devices with different channel lengths and widths, we introduce a parameter $\eta \equiv A_N L^2/R$ to describe the noise magnitude. From eq 2, it is straightforward to show that η provides a convenient metric to measure the material-specific $1/f$ noise level independent of device geometry, and in SLG devices, $\eta = e\mu\alpha_H$ is directly related to Hooge's parameter. Figure 4 plots the noise factor η as a function of unit-length resistance (R/L) for two SLG and three BLG devices with various channel dimensions. We find that the two SLG devices yield a constant η with comparable magnitudes, within a factor of 2, as a function of resistance, suggesting the same Hooge's parameter $\sim 10^{-3}$ for both samples. On the other hand, the noise factor η of all the BLG devices shown in Figure 4 exhibits a strong dependence on resistance, where η increases with decreasing R. The minimal η of the BLG devices, which is more than one order of magnitude lower than those of SLG devices, occurs at the Dirac point corresponding to R_{max}. In Figure 4, it is interesting to note that the noise factor η of all BLG devices, despite their different dimensions, seems to asymptotically reach the same value as $R \rightarrow 0$ and can be phenomenologically fitted by

$$\eta \sim \eta_0 \exp\left(-g\frac{R}{R_{max}}\right) \quad (3)$$

where η_0 is the constant noise factor in SLG and g is a constant.

Qualitatively, the asymptotic behavior of eq 3 suggests that, in both monolayer and bilayer systems, the $1/f$ noise is due to the same fluctuation mechanism, i.e., interaction between oxide surface and the adjacent graphene layer. In order to evaluate possible causes for the distinct gate dependence and noise amplitude observed in SLG and BLG nanodevices, we first consider the carrier concentration and charge distribution in graphene bilayers under the influence of a gate field. The total carrier concentration n induced by the applied gate voltage in an undoped graphene device is determined by $n = C_g V_g/e$, where C_g is the gate capacitance consisting of the quantum capacitance C_Q and the electrostatic capacitance C_e in series, i.e., $C_g^{-1} = C_Q^{-1} + C_e^{-1}$. For a typical carrier density of $n \sim 10^{12}$ cm^{-1}, C_Q is on the order of 10^{-5} F/cm^{-2} for both graphene monolayers[24] and bilayers, i.e., much larger than the electrostatic capacitance $C_e \simeq 10^{-8}$ F/cm^{-2} for 300 nm thick SiO_2 dielectrics used here. Thus, for both types of devices studied here, the gate capacitance C_g is dominated by the electrostatic capacitance C_e, and the total carrier concentration is given by $n = \gamma V_g$ ($\gamma \approx 7.2 \pm 10^{10}$ cm^{-2}/V)[3,6] as mentioned earlier. In graphene bilayers, we denote by n_1 and n_2 the carrier density in the bottom (closer to the oxide) and the top (facing vacuum) layers, respectively, and $n = n_1 + n_2$. In the absence of screening, the two layers possess equal charge density $n_1 = n_2 = n/2$, whereas in the case of perfect screening by the bottom layer, we have $n_1 = n$ and $n_2 \simeq 0$. In reality, since the screening length of graphite in the c-axis is $\sim$5 Å,[25] comparable to the interlayer distance $\sim$3.4 Å, the actual charge distribution is between the two extremes,[26] and we have $n_1 = n/2 + \Delta/2$ and $n_2 = n/2 - \Delta/2$, where $\Delta = n_1 - n_2$ is the charge imbalance due to the screening. It is important to point out that while it may seem intuitive to view the bilayer system as a parallel-plate capacitor and attribute the lower noise level η in BLG devices to the charge distribution $n_1 < n$, a closer examination of this simple electrostatic screening model reveals significant discrepancy, both qualitative and quantitative, between the predicted noise behavior and the experimental results shown in Figure 4, as explained here. Assuming a noiseless transport behavior for carriers residing on the *top* graphene layer and similar fluctuations experienced by carriers in the *bottom* layer as those in SLG, the noise factor of the BLG can be written as $\eta = (n_1/n)\eta_0$ in the context of Hooge's noise relation. It can be readily seen that this simple model yields a lowest possible noise factor of only $\sim\eta_0/2$ for graphene bilayers in the absence of screening ($n_1 = n_2$), and this value is orders of magnitude larger than our measured results (see Figure 4). Furthermore, McCann has calculated the carrier density inhomogeneity in graphene bilayer using a self-consistent tight-binding model and the Hartree approach[1] and showed that as V_g varies, the charge density n_1 (or n_2) exhibits a quasi-linear dependence on the total carrier density n (up to $n \leq 10^{13}$ cm^{-2}). On the basis of the simple screening model, this linear dependence of n_1 and n_2 on n would lead to a noise factor η that is roughly constant as a function of V_g, which is also inconsistent with the trends observed in Figure 4.

In light of the inadequacy of the simple capacitor model that only considers the effect of the charge distribution under a given external field, we conclude that the anomalous noise behavior observed in BLG devices must be associated with the coupling between the two layers that gives rise to a unique field-dependent band structure in graphene bilayers.

Both theoretical[1] and experimental studies have shown that an energy gap Δ_g between the conduction and valence band can be induced in graphene bilayers by doping[2] or applying a gate field.[26,27] For undoped devices, the band gap Δ_g is found to linearly increase with the charge concentration n,[1] yielding $\Delta_g \sim 10$ meV for $n \sim 10^{12}$ cm^{-2}. Therefore, for our BLG devices, the band gap Δ_g is proportional to the gate voltage V_g, $\Delta_g/V_g \simeq 13.9$ (meV/V), and at $V_g = \pm 20$ V, the field-induced band gap is estimated to be $\Delta_g \simeq 28$ meV. We note that in the nanoribbon devices, a band gap $\Delta_Q = 2\hbar^2/(2m_eW^2)$ can also be produced by quantum confinement effects, where m_e is the electron effective mass. To evaluate Δ_Q in BLG nanoribbon devices, we take $m_e = 0.05\ m_o$ (m_o is the free electron mass), which is the lower limit of measured cyclotron mass of electrons in graphene bilayers,[1,26] and obtain $\Delta_Q \sim 0.7$ meV for $W = 30$ nm, indicating that this size-induced band gap is negligible compared to the gate-induced Δ_g in our BLG devices for most Δ_g. Similarly in SLG nanodevices, there may also exist a size-dependent band gap due to quantum confinement, which can be as large as 20 meV for a 30 nm wide ribbon.[10] We note that this band gap in SLG devices, while independent of the gate field, is found to be highly sensitive to the exact channel edge configurations (i.e., zigzag vs armchair).[8] Nevertheless, both previous noise studies on SLG nanoribbons[9] and our results here (Figure 4) reveal that the noise amplitude α_H in SLG devices is not affected by this size-induced band gap as a function of device W down to 20 nm, and therefore, the SLG nanoribbon can be treated as a regular semiconductor in this context.

On the basis of the above findings, a qualitative understanding of the data shown in Figure 4 emerges. First, since 1/*f* noise mainly originates from the fluctuating trap charges in the oxide that modulate the carrier mobility in the channel, the noise amplitude is highly dependent on the effectiveness of the impurity charge screening in the channel. In a graphene monolayer, the in-plane screening of an external impurity charge is found to exhibit a slow algebraic decay with a characteristic length of 3.8 Å due to both the Dirac-like dispersion relation and its two-dimensional nature.[28] In graphene bilayers, we expect this screening to be much stronger due to a more *bulk*-like character, as implied by a comparable screening length in the *c*-axis, as well as the parabolic band-structure distinct from that of graphene monolayers. More importantly, in narrow gap semiconductors, the screening strength diminishes with increasing bandgap, and therefore, the mobility fluctuation due to the same trap charge perturbation is expected to become larger as Δ_g increases, consistent with the trend observed in Figure 4 that exhibits a minimal noise factor η at the Dirac point. This gate-dependent (or gap-dependent) screening property in graphene bilayers is also reflected in the ab initio calculation by Min et al.[29] where it is found that as Δ_g approaches 0, the ratio between the induced channel potential variation and the external perturbing potentials also vanishes. We believe that the low noise level observed in the BLG, especially near the Dirac point, is related to this dynamic charge redistribution that provides effective screening to the nearby trap charges in the oxide. A detailed theoretical model for BLG that considers the self-consistent charge distribution and the impact of screening on Columb scatters in the oxide is, however, required in order to provide quantitative insight into the suppressed 1/*f* noise in the bilayer graphene system.

In summary, we have performed 1/*f* noise measurements on both single-layer and bilayer graphene nanodevices, revealing distinct noise characteristics for the two systems. The 1/*f* noise in graphene monolayers is found to follow Hooge's empirical relation, yielding a noise level per carrier comparable to carbon nanotube devices and bulk semiconductors despite its 2D nature. Unexpectedly, the 1/*f* noise level in graphene bilayers is strongly suppressed compared to their monolayer counterparts and also exhibits an unusual dependence on the carrier density in contrast to other known materials. This unique 1/*f* noise behavior observed in graphene bilayers is likely associated with a band structure that depends on the charge distribution among the two layers, resulting in an effective screening of scattering due to external impurity charges. Nevertheless, both graphene monolayer and bilayer devices exhibit 1/*f* noise levels independent of carrier type. While further detailed quantitative analysis and studies are required to understand these phenomena, the findings here provide exciting opportunities for graphene bilayers in low-noise applications.

Methods. Ultrathin graphite films containing few-layer graphene were obtained by mechanical exfoliation and transferred to a highly doped Si substrate covered with 300 nm thick SiO_2. The absolute number of graphene layers is determined by atomic force microscopy height measurements to identify single-layer and bilayer graphene domains. To fabricate graphene nanodevices, Pd contacts are first deposited as the source and drain electrodes by e-beam lithography and lift-off. Narrow ribbons of graphene between the metal contacts are formed by oxygen plasma RIE etching using a patterned HSQ (hydrogen silsesquioxane) layer as the protective mask. Finally, the HSQ layer is removed in buffered HF solution. All the electrical measurements in this report were performed under high vacuum ($\sim 10^{-7}$ Torr) at room temperature.

Acknowledgment. The authors are indebted to Z. Chen for assistance with graphene device fabrication and V. Perebeinos for useful discussions. We also thank B. Ek for expert technical assistance.

References

(1) McCann, E. *Phys. Rev. B* **2006**, *74*, 161403R.
(2) Ohta, T.; Bostwick, A; Seyller, T.; Horn, K.; Rotenberg, E. *Science* **2006**, *313*, 951.
(3) Zhang, Y; Tan, J. W.; Stormer, H. L.; Kim, P. *Nature* **2005**, *438*, 201.
(4) Geim, A. K.; Novoselov, K. S. *Nat. Mater.* **2007**, *6*, 183.
(5) Avouris, P.; Chen, Z.; Perebeinos, V. *Nat. Nanotechnol.* **2007**, *2*, 605.
(6) Novoselov, K. S; Geim, A. K.; Morozov, S. V; Jiang, D.; Katsnelson, M. I; Grigorieva, I. V.; Dubonos, S. V.; Firov, A. A. *Nature* **2005**, *438*, 197.
(7) Berger, C.; Song, Z.; Li, X; Wu, X; Brown, N; Naud, C.; Mayou, D.; Li, T; Hass, J.; Marchenkov, A. N. *Science* **2006**, *312*, 1191.
(8) Nakada, K; Fujita, M.; Dresselhaus, G.; Dresselhaus, M. S. *Phys. Rev. B* **1996**, *54*, 17954.
(9) Chen, Z; Lin, Y.-M.; Rooks, M. J.; Avouris, P. *Physica E* **2007**, *40*, 228.

(10) Han, M. Y.; Ozyilmaz, B.; Zhang, Y.; Kim, P. *Phys. Rev. Lett.* **2007**, *98*, 206805.
(11) Chen, J. H.; Jang, C.; Fuhrer, M. S.; Williams, E. D.; Ishigami, M. Cond-mat/0708.2408.
(12) Ando, T. *J. Phys. Soc. Jpn.* **2006**, *75*, 074716.
(13) Schedin, F.; Geim, A. K.; Morozov, S. V; Hill, E. W; Blake, P; Katsnelson, M. I.; Novoselov, K. S. *Nat. Mater.* **2007**, *6*, 652.
(14) Razavi, B. *IEEE J. Solid-State Circuits* **1996**, *31*, 331–343.
(15) Lin, Y.-M.; Appenzeller, J; Knoch, J.; Chen, Z.; Avouris, P. *Nano Lett.* **2006**, *6*, 930.
(16) Ishigami, M.; Chen, J. H; Williams, E. D; Tobias, D.; Chen, Y. F.; Fuhrer, M. S. *Appl. Phys. Lett.* **2006**, *88*, 2031116.
(17) Kim, S. K.; Xuan, Y; Ye, P. D.; Mohammadi, S.; Back, J. H.; Shim, M. *Appl. Phys. Lett.* **2007**, *90*, 163108.
(18) Lin, Y.-M; Appenzeller, J.; Chen, Z; Avouris, P. *Physica E* **2007**, *37*, 72.
(19) Lin, Y.-M; Tsang, J. C; Freitag, M.; Avouris, P. *Nanotechnology* **2007**, *18*, 295202.
(20) Koshino, M.; Ando, T. *Phys. Rev. B* **2006**, *73*, 245403.
(21) Cserti, J.; Csordas, A.; David, G. *Phys. Rev. Lett.* **2007**, *99*, 066802.
(22) Hooge, F. N. *Phys. Lett.* **1969**, *29A*, 139.
(23) Appenzeller, J.; Knoch, J.; Derycke, V; Martel, R.; Wind, S.; Avouris, P. *Phys. Rev. Lett.* **2002**, *89*, 126801.
(24) Guo, J.; Yoon, Y.; Ouyang, Y. *Nano Lett.* **2007**, *7*, 1935.
(25) Pietronero, L.; Strassler, S.; Zeller, H. R.; Rice, M. J. *Phys. Rev. Lett.* **1978**, *41*, 763.
(26) Castro, E. V; Novoselov, K. S; Morozov, S. V; Peres, N. M. R; dos Santos, J. M. B. L; Nilsson, J; Guinea, F; Geim, A. K.; Neto, A. H. C. *Phys. Rev. Lett.* **2007**, *99*, 216802.
(27) Oostinga, J. B.; Heersche, H. B.; Liu, X; Morpurgo, A. F.; Vandersypen, L. M. K. *Nat. Mater.* **2008**, *7*, 151.
(28) DiVincenzo, D. P.; Mele, E. J. *Phys. Rev. B* **1984**, *29*, 1685.
(29) Min, H.; sahu, B.; Banerjee, S. K.; MacDonald, A. H. *Phys. Rev. B* **2007**, *75*, 155115.

NL080241L